Analysis of Fracture Mechanism
of Cast Steel for Different States of Stress

J. Lachowski *, J. Borowiecka-Jamrozek
Kielce University of Technology,
Al. Tysiąclecia PP. 7, 25-314 Kielce, Poland
* Corresponding author. E-mail address: jlach@tu.kielce.pl

Abstract

In this paper a plastic deformation and a damage evolution in low-carbon cast steel containing non-metallic inclusions are analysed experimentally and numerically. Two microstructures of the cast steel have been obtained after appropriate heat treatment. Tensile tests of smooth specimens and axisymmetric notched specimens have been performed. The notched specimens have the notch radii: 1 mm, 3 mm and 7 mm. Fractography of the specimens was carried out to observe fracture mechanisms. The mechanism depended on the stress state in the notched specimens. The fractography showed the existence of two fracture mechanisms: ductile failure and by shear.

The process of the voids growth formed on the non-metallic inclusions was the process which included in the explanation of the damage mechanism. Modelling of deformation of the specimens has been used with the model suggested by Gurson, Tvergaard and Needleman. The model is implemented in the Abaqus finite element program. The computer simulation was performed using ABAQUS system. The computed output was compared with the experimental results obtained for specimens of the same shape.

Keywords: Metallography, Mechanical properties, Cast steel, Damage evolution, Computer modelling

1. Introduction

In metallic materials, plastic deformation and failure mechanisms depend on the stress state. It is known that inclusions play a significant role in the deformation, damage and failure of such materials. In metallic materials, voids nucleation and growth depend on the stress state [1].

In engineering analysis the Mises yield criterion is mainly applied and the materials are considered as isotropic ones. The influence of inclusions and microvoids on plastic deformation and fracture mechanism has been taken into account in model suggested by Gurson [2] as well as Tvergaard and Needleman [3,4] (GTN model).

2. Experimental results

Experiments have been performed on a low-carbon cast steel. The chemical composition of the material was presented in the tab. 1.

Table 1.
Chemical composition (wt%)

C	Mn	Si	P	S	Cr	Ni	Mo
0.21	0.38	0.32	0.021	0.042	0.74	0.085	0.42

The cast steel was subjected to the two heat treatment: cast steel type I - normalising at 920°C, 2 h, oil quenching and tempering at 490°C, 2 h; cast steel type II - normalising at 920°C, 2 h, oil quenching and tempering at 350°C, 0.5 h. As the result a ferritic-pearlitic structure of the material was obtained (Fig. 1).
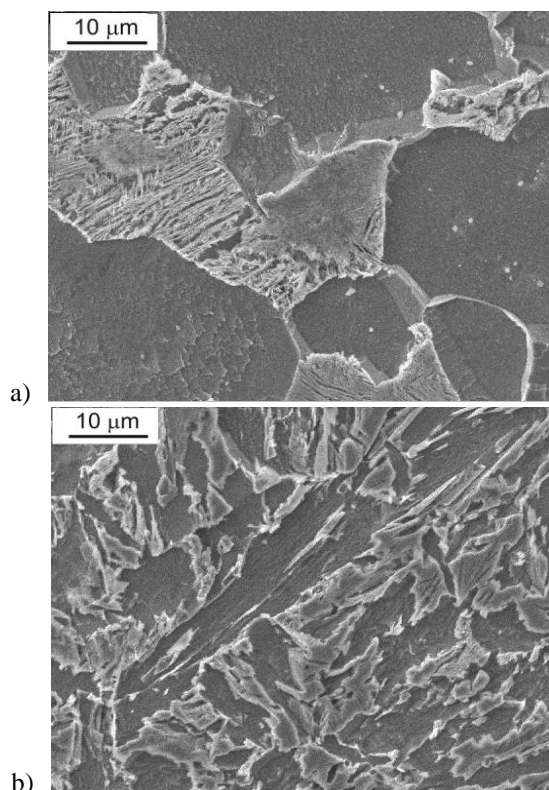
a)

b)

Fig. 1. Microstructure of the cast steel, a) type I, b) type II

The uniaxial tensile tests of the materials were carried out on three specimens with a diameter of 6 mm. The specimens were selected from materials obtained by two methods of heat treatment (Fig.1). The yield stress, the tensile strength and the elongation were determined in the tests (Tab. 2).
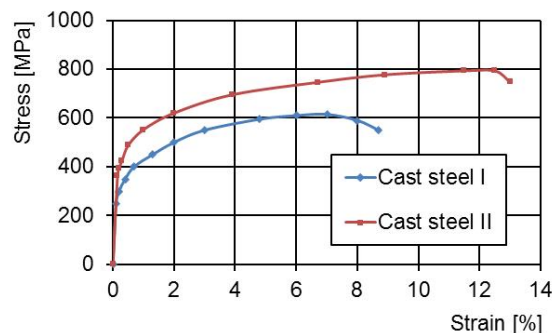

Fig. 2. Stress-strain relation of cast steel I (red curve) and cast steel II (blue curve)

The stress triaxiality factor T, which characterize the stress state, is a non-dimensional mechanical parameter defined as the ratio of the mean stress and the equivalent stress

$$T = \frac{\sigma_m}{\sigma_{eq}} \qquad (1)$$

Table 2.
Mechanical parameters

Material	Elastic modulus E, GPa	Poisson ratio ν	Yield stress $R_{p0,2}$, MPa	Tensile strength R_m, MPa	Elongation A, %
Cast steel I	213	0,28	283	615	8.7
Cast steel II	212	0,28	364	793	13.0

To analyze mechanisms of failure, the samples were examined under different triaxial states of stress. These stress states were obtained in tensile testing on specimens with different notch radii. The tensile tests were performed on notched specimens with outside diameter equal to 14 mm and diameter at the minimal cross-section equal to 7 mm. The specimens had notch radii of 1 mm, 3mm and 7 mm (Fig. 3).
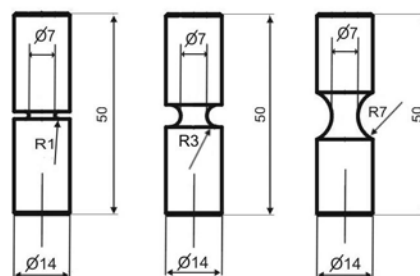

Fig. 3. Notched specimens, notch radius equal to 1 mm, 3 mm and 7 mm, dimensions given in mm

This stress triaxiality factor at the minimal cross-section of applied samples is defined by the equation [5, 6]

$$T = \frac{1}{3} + \ln\left(\frac{r_0^2 + 2r_0\rho - r_1^2}{2r_0\rho + 1} \right) \qquad (2)$$

where r_0 is the minimal cross-section radius, ρ is the notch radius and r is the distance from centre of the sample. The T factor is the greatest in the centre of the sample and decreases along the sample radius.

Thus different stress triaxiality in the centre of sample has been considered. The initial values of the factor T in the experiment and in the simulation were: 1.34 (ρ = 1 mm), 0.79 (ρ = 3 mm) and 0.56 (ρ = 7 mm). Stress triaxiality factor at the surface of the notch of the sample is equal to 0.33.

During the tensile test carried out on notched specimens, the loading force was recorded as a function of the change in the minimal diameter of the cross-section of the samples. The measurement was made with the help of a special clip extensometer. The value of the average reduced strain was calculated from the change of sample diameter using the formula:

$$\varepsilon = 2 \cdot \ln\left(\frac{d_0}{d}\right) \qquad (3)$$

where d_0 is the initial diameter and d is an actual diameter at minimal section of the notched specimen. Typical relationship between stress and strain in the neck of a specimen is shown in Fig. 4 and Fig. 5.
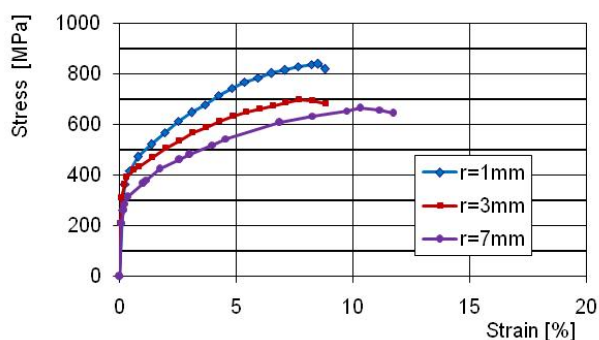

Fig. 4. Stress-strain curve for the notched specimens, cast steel I
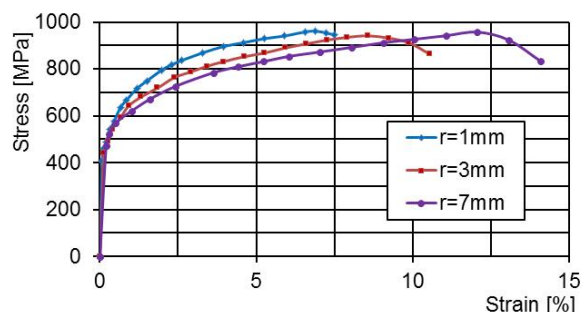

Fig. 5. Stress-strain curve for the notched specimens, cast steel II

3. Fractography

The fractographic examination showed the relation between the fracture morphology and the stress state. These examination indicated that stress state influenced the fracture surface morphology. The morphology of the fracture surfaces in the center and near the edges of the samples were taken.

It was assumed that the stress triaxiality factor is the parameter which controls the fracture process. The fracture mechanism was analyzed in dependence on the triaxiality of the stress at the neck of samples. The stress triaxiality decreases along the sample radius from centre to the surface. Two failure mechanisms occur in a sample: ductile failure in the centre and shear at the surface of a sample. Voids nucleation at non-metallic inclusions coalescence of the voids preceded the ductile fracture.

Typical fracture surface morphology are shown in Figs 7-10. The morphology changes from the center to the edge of the sample. Figure 7a shows the centre of sample from cast steel I with notch radius $r = 1$ mm. The nucleation of voids at non-

metallic inclusions is the beginning of ductile fracture. The fracture surface indicates that the voids growth causes the appearance of dimples in the centre of the samples.

In Figure 7b , the surface of a specimen is presented. In the specimen with the notch radius 7 mm, the stress triaxiality factor changes from 0.54 in the centre of the specimen to 0.33 at the surface (Fig. 7b) and shear fracture is dominant, but a few dimples are visible.
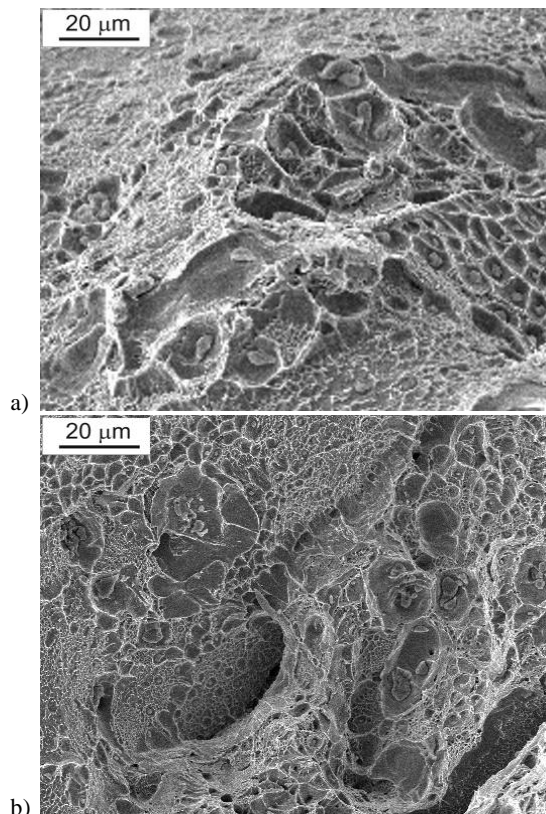

a)

b)

Fig. 7. Tensile test of material type I, notch radius $r = 1$ mm, a) ductile fracture at centre of specimen, b) shear fracture at surface of specimen

High triaxial stress accelerates the growth of voids nucleated at non-metallic inclusions and leads to ductile fracture. Large dimples, which are shown in the centre of the specimens are the result of the growth and coalescence of voids (Fig. 8a).
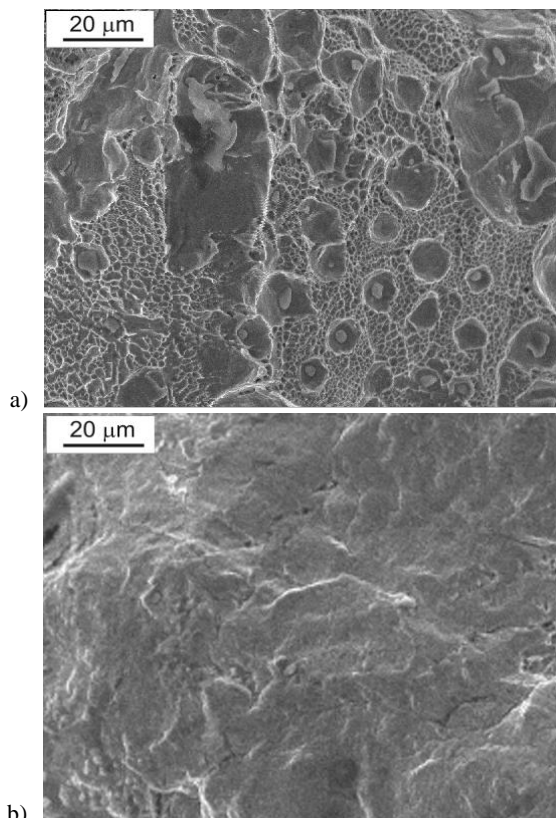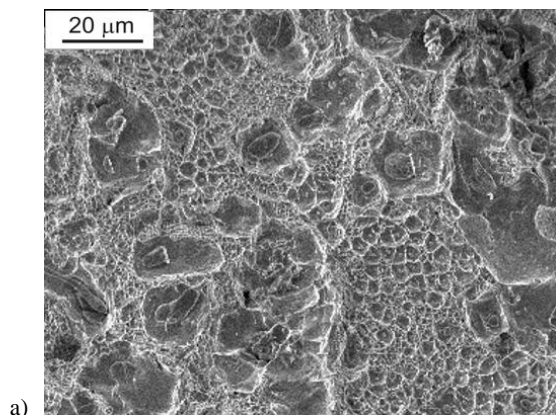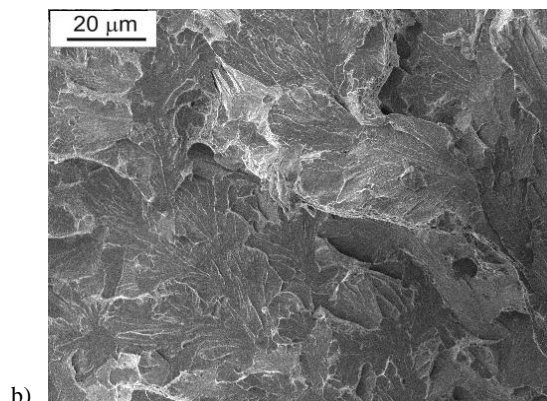
a)

b)

Fig. 9. Tensile test of material type II, notch radius r = 1 mm, a) ductile fracture at centre of specimen, b) shear fracture at surface of specimen

a)

b)

Fig. 8. Fig. 8. Tensile test of material type I, notch radius r = 7 mm, a) ductile fracture at centre of specimen, b) shear fracture at surface of specimen
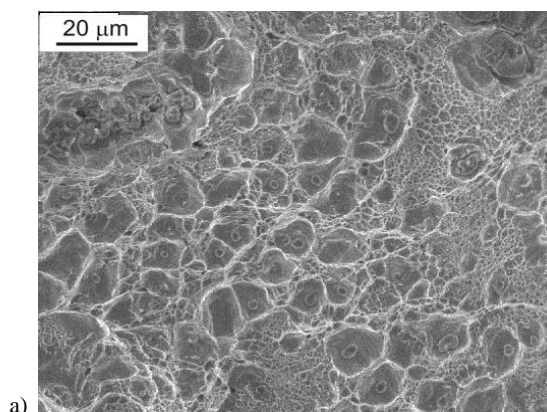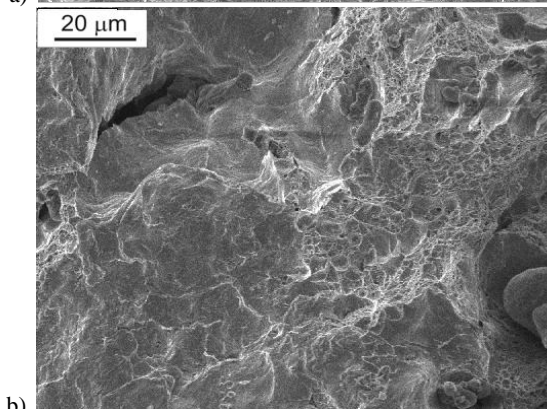

a)

a)

b)

Fig. 10. Tensile test of material type II, notch radius r = 7 mm, a) ductile fracture at centre of specimen, b) shear fracture at surface of specimen

The inclusions on the surface of fractures were investigated with the X-ray testing. Manganese sulphides and iron sulphides are the main identified inclusions. The manganese sulphide inclusion was presented in Fig. 11.
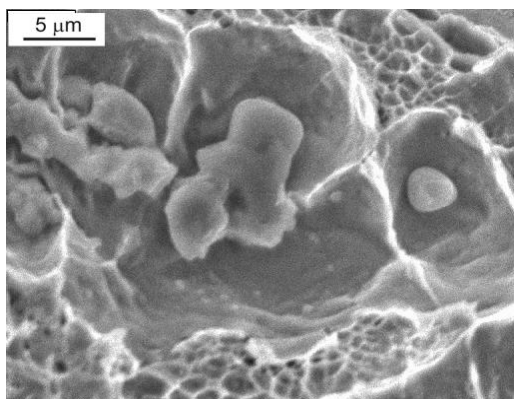
Fig. 11. The identified inclusion of manganese sulfide

4. Model of plastic deformation of a metal with voids

The Gurson-Tvergaard-Needleman constitutive equation (GTN model) for a metal containing voids is as follows [7]

$$\Phi = \frac{\sigma_{red}^2}{\sigma(\varepsilon)^2} + 2q_1 f^* \cosh\left(-q_2 \frac{3\sigma_m}{2\sigma(\varepsilon)}\right) - \left(1 + \left(q_1 f^*\right)^2\right) = 0 \qquad (4)$$

where σ_{red} is the Huber-Mises reduced stress, σ_m is the mean stress, and $\sigma(\varepsilon)$ is the stress according to the actual stress-strain curve (Fig. 2). The q_i parameters are coefficients characterizing the plastic properties of a metal [8,9]. For the calculations, the parameters, $q_1 = 1.5$ and $q_2 = 1$, were chosen [3,4]. Function f^* defines a rapid reduction in the load transmitted through material with increasing void volume fraction f

$$f^*(f) = f \qquad for\, f \leq f_c \qquad (5a)$$

$$f^*(f) = f_c + \frac{1 - f_c}{f_F - f_c}\left(f - f_c\right) \qquad for\, f > f_c \qquad (5b)$$

where f is the void volume fraction, f_c is the critical value of the void volume fraction (at the point the process of void nucleation begins and the strength of the material decreases rapidly. Parameter f_F is the void volume fraction which initiates fracture. When $f^*=0$ equation reduces to the Huber-Mises flow criterion [8-10].

In the GTN model it has been assumed that an increase of the void volume fraction with increasing plastic strains occurs as a result of the growth of voids present in the metal and voids generated on inclusions (decohesion on the particle-matrix border) [4].

$$df = df_g + df_n \qquad (5)$$

where df_g - is an increase in the volume fraction of voids present in the material, df_n - is an increase in the volume fraction of voids generated during the plastic deformation. In numerical modelling, the nucleation of new voids was determined using the following formula

$$df_n = A \cdot d\varepsilon^{pl} \qquad (5)$$

where coefficient A represents the voids nucleation with the normal distribution around a certain value of the mean strain [4,11]

$$A = \frac{f_N}{s\sqrt{(2\pi)}} \exp\left[-\frac{1}{2}\left(\frac{\varepsilon - \varepsilon_N}{s_N}\right)^2\right] \qquad (6)$$

where f_N represents the volume fraction of void which are nucleated at non-metallic particles, ε_N is the mean plastic strain of void nucleation, and s_N is the standard deviation of nucleation.

The GTV model has been implemented in the Abaqus finite element software [11]. The Abaqus program has been used to performed the simulation of the deformation and damage of the cast steel.

5. Computer simulation results

The above simulation model for a material containing voids and inclusions on which voids form was used to explain the failure process at the spatial stress state. The theoretical stress-strain relation has been obtained taking into consideration the parameters presented in Table 3. The best results were obtained for the values of the parameters.

Table 3.
Material parameters used in the computer simulation

f_0	f_N	ε_N	s_N	f_C	f_F
0.0	0.005	0.01	0.005	0.025	0.25

The plastic equivalence strain (PEEQ) [11] changes distinctly along radius of a minimal cross-section of a sample (Fig. 12 and Fig. 13). So that the formula (3) gives only approximate and average value.
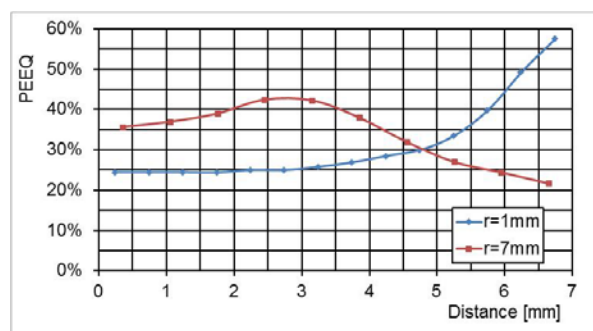

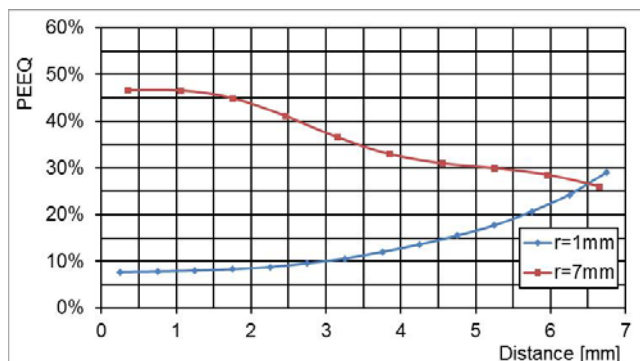Fig. 12. Computer-simulated of the effective strain across the neck section for the cast steel I

Fig. 13. Computer-simulated of the effective strain across the neck section for the cast steel II

The voids volume fraction (VVF) for the samples with notch radius 1 mm and 7 mm are presented in Fig. 14 and Fig. 15. The void volume fraction at failure point is about 20-25% in the centre of neck. In the case of the border the VVF is small and does not exceed the value of 2.5% (Fig. 14 and 15).
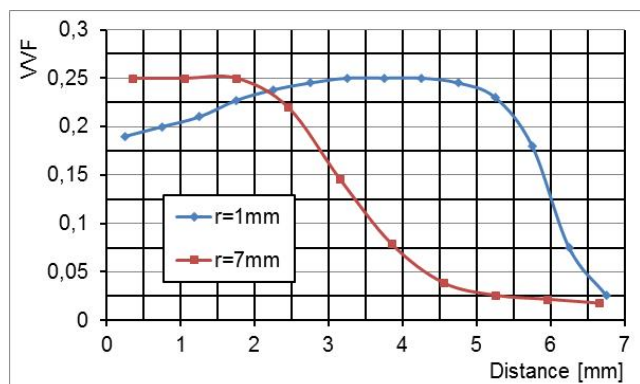

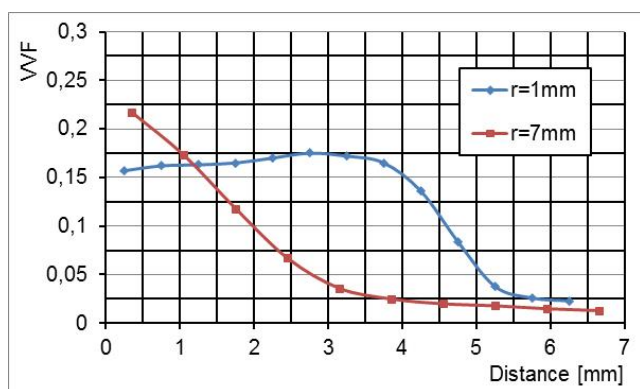Fig. 14. Void volume fraction across notch section for the specimens of cast steel I

Fig. 15. Void volume fraction across notch section for the specimens of cast steel II

Conclusions

The two tested cast steels have been analyzed in different states of stress. The observed fracture mechanisms in the materials depend on the state of stress. In the centre of the notched specimens the stress triaxiality was large. So that ductile fracture was observed in the centre. At the surface of the notched specimen the stress triaxiality was less and fracture by shear was dominant. At the centre of the samples the initiation of the void coalescence process was take place before faluire.

References

[1] Lachowski, J. & Biel-Gołaska M. (2000). Modelling of Damage Evolution in Cast Steel, Conference Advances in Mechanical Behaviour, Plasticity and Damage EUROMAT 2000, 7-9 November, pp. 1457-1462, Tours, France.

[2] Gurson, A.L. (1977). Continuum theory of ductile rupture by void nucleation and growth. *Journal of Engineering Materials Technology*. 99, 2-15.

[3] Tvergaard, V. & Needleman, A. (1984). Analysis of the cup-cone fracture in a round tensile bar. *Acta Metallurgica*. 32(1), 157-169.

[4] Needleman, A. & Tvergaard, V. (1984). An analysis of ductile rupture in notched bars. *Journal of Mechanics and Physics of Solids*. 32(6), 461-490.

[5] Bridgman, P.W. (1952). *Studies in Large Plastic Flow and Fracture*. Harvard University Press, Cambridge, Massachusetts, Chapter 1.

[6] Biel-Gołaska, M. & Gołaski, L. (1994). The analysis of the ductile failure process of cast steel subjected to triaxial stress states, Foundry Reaserch Institute, Cracow, XLIV, No 1-2, pp. 37-57.

[7] Borowiecka-Jamrozek, J., Lachowski, J. (2014). An analysis of stresses in an Al-5%Si alloy under load, Conference "Recent Trends in Structural Materials", COMAT 2014, Nov. 19-21, pp. 6. Pilzen, Czech Republic.

[8] Koplik, J. & Needleman, A. (1988). Void coalescence in porous plastic solids. *International Journal of Solids Structures*. 24(8), 835-853.

[9] Richelsen, A.B. & Tvergaard, V. (1994). Dilatant plasticity or upper bound estimates for porous ductile solids. *Acta metall materialia*. 42(8), 2561-2577.

[10] Tvergaard V. (2001). Crack growth predictions by cohesive zone model for ductile fracture. *Journal of Mechanics and Physics of Solids*. 49, 2191-2207.

[11] SIMULIA Dassault System, *Abaqus analysis user's manual, Version 6.12* , 2017.